Chemistry–A European Journal
Review
doi.org/10.1002/chem.202200843
Chemistry Europe
European Chemical Societies Publishing
www.chemeurj.org

Muon Spin Rotation/Resonance (μSR) for Studying Radical Reactivity of Unsaturated Organophosphorus Compounds

Shigekazu Ito*[a]

Dedicated to Professor Masaaki Yoshifuji on the occasion of his 80th birthday.

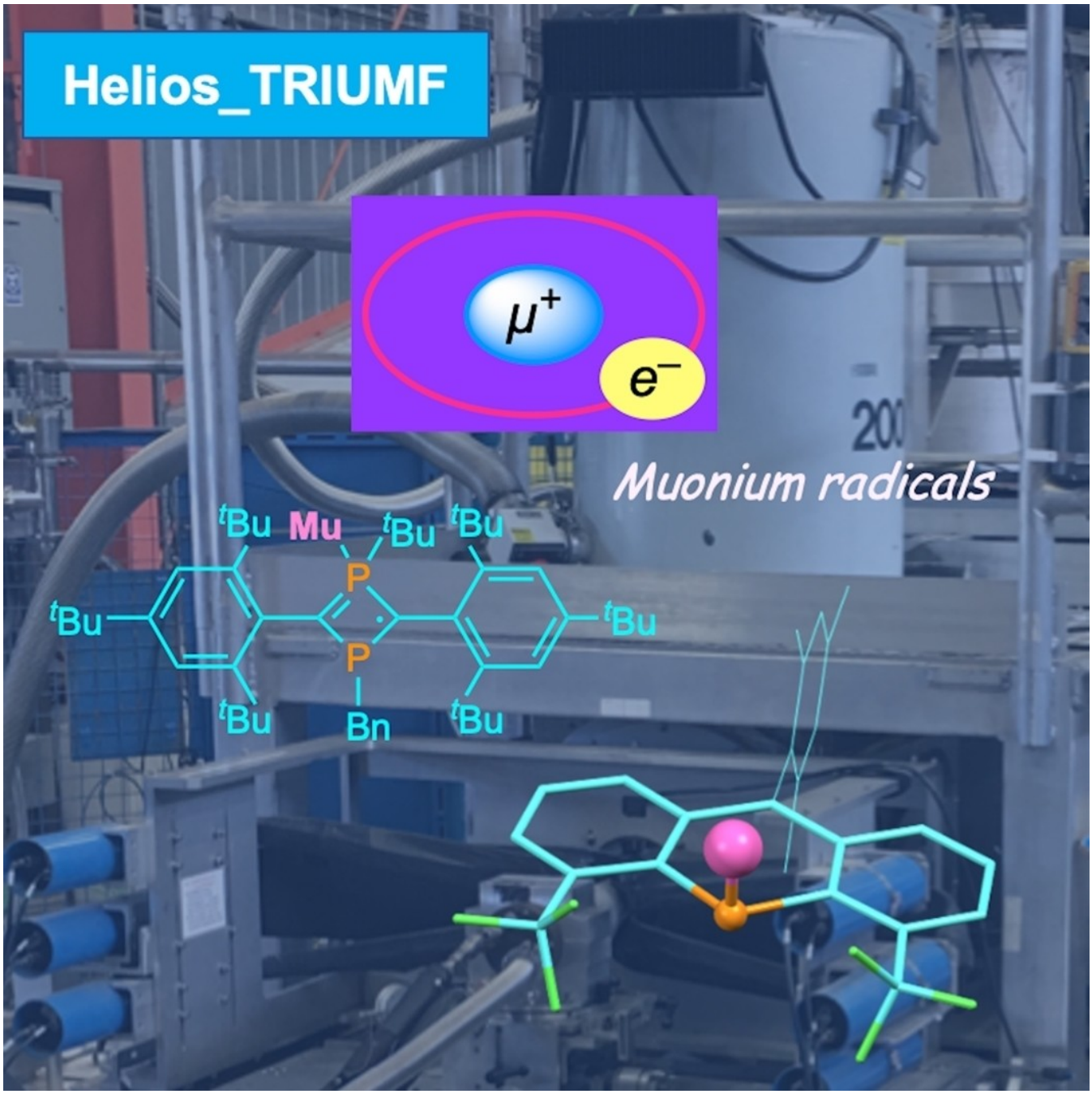

Abstract: The positive muon (μ^+) can be regarded as a light isotope of proton and has been an important tool to study radical reactions of organic compounds. Recently, muons have been applied to produce short-lived paramagnetic species from the heavier unsaturated organic molecules including the p-block elements. This article overviews recent muon spin rotation/resonance (μSR) studies on the phosphorus analogs of alkenes, anthracenes, and cyclobutane-1,3-diyls together with the fundamentals of μSR. The acyclic phosphaalkene of P=C and phosphasilenes of P=Si can accept muonium (Mu = [μ^+e^-]) at the heavier double bonds, and the corresponding radicals have been characterized. The phosphorus atom in 9-phosphaanthracene, whose P=C double bond is stabilized by the *peri*-substituted CF_3 groups, predominantly captures muonium to provide the corresponding paramagnetic fused heterocyclic system. The *peri*-trifluoromethyl groups are functional to promote the unprecedented light isotope effect of muon providing the planar three-cyclic molecular structure to consume the increased zero-point energy. The formally open-shell singlet 1,3-diphosphacyclobutane-2,4-diyl unit can accept muonium at the (ylidic) phosphorus or the skeletal radicalic carbon, and the corresponding paramagnetic phosphorus heterocycles can be characterized by μSR. The findings on these muoniation processes to the unsaturated phosphorus-containing compounds will contribute not only to development of novel paramagnetic functional species but also to progress on muon science.

1. Introduction

The positive muon is a subatomic particle and is classified as a lepton. In nature, the muons are produced by the reaction of cosmic rays with high energy protons and molecules in the earth's upper atmosphere. For materials science, using accelerators such as cyclotrons and synchrotrons is appropriate because beams of muons of sufficient intensity to analyze the physical characteristics (within a reasonable amount of time) can be produced. Both positive and negative muons can be produced from accelerators, but in most cases positive muons are employed for muon spin rotation/resonance (μSR) experiments for materials research. As described in the previous publications,[1–4] the μSR technique can be utilized as a powerful analytical method for radical reactions of organic molecules. The spectroscopic technique using the spin-polarized muon is similar to nuclear magnetic resonance (NMR) and electron-spin resonance (ESR).

A nuclear reaction of a high-energy beam of proton from accelerator facilities providing the pi meson (pion, π^+) is shown in Equation (1). The average lifetime of pion is 26 ns, and subsequently the positive muon (μ^+) is produced together with muon-neutrinos (ν_μ). The muon is a particle with a mass one ninth that of proton (0.113 amu), spin of 1/2, and average lifetime of $\tau_\mu = 2.2$ μs. The muon spin must be opposite to the neutrino spin to conserve momentum from pions of zero spin, and accordingly the muons obtained in accelerator factories are almost 100% spin-polarized. The polarization of the ensemble of μ^+ is quite useful for the magnetic spectroscopic studies with high time resolution because there is no need to first create spin coherence using a high frequency preparation pulse. Typical properties of proton, muon, and electron are summarized in Table 1. Besides the light mass of muon compared with proton, it is important for discussing the spectroscopic parameters, notably hyperfine coupling (hfc) constants, that the magnetic moment of muon is 3.1833 times that of proton.

$$\pi^+ \rightarrow \mu^+ + \nu_\mu \quad (1)$$

Muons, produced by accelerators, are implanted into the material with an energy of 4 MeV, and lose energy in 0.1–1 ns to a few keV by ionization of atoms and scattering with electrons. The stopping range of the 4 MeV muon energy is 0.15 ± 0.01 gcm^{-3}, corresponds a penetration depth of ca. 0.2 mm in copper, 1.5 mm in water, or 1 m in helium gas at STP (standard temperature and pressure).[3a] Figure 1 illustrates the nature of the final muon states. In contact with insulators (solid, liquid, and gas) or semiconductors, the positive muon can capture an electron and become a muonium (Mu = [μ^+e^-]) that can be regarded as a light isotope of neutral hydrogen atom. The muonium can be stable at the energy below 13.54 eV of the ionization energy, and the hfc is 4463.3 MHz. The H-atom surrogate can add to the unsaturated molecular units and provide the corresponding transient paramagnetic species. In

Table 1. Properties of proton, muon, and electron.

	H^+ (p)	μ^+	e
charge	$+e$	$+e$	$-e$
spin	1/2	1/2	1/2
mass	1.6726×10^{-27} kg $= m_p$	$0.1126m_p$	$m_p/1836.2$
gyromagnetic ratio/(2π)	4.2577 kHz G^{-1}	13.55342 kHz G^{-1}	2802.421 kHz G^{-1}
magnetic moment	1.4106×10^{-26} J T$^{-1} = \mu_p$	$3.1833\mu_p$	$-658.21\mu_p$
g factor	5.5857	2.0023	−2.0023
lifetime	$>2\times10^{26}$ y	2.2×10^{-6} s	$>4\times10^{23}$ y

[a] *Prof. Dr. S. Ito*
Department of Applied Chemistry,
School of Materials and Chemical Technology
Tokyo Institute of Technology
2-12-1-H113 Ookayama, Meguro-ku, Tokyo 152-8552 (Japan)
E-mail: ito.s.ao@m.titech.ac.jp

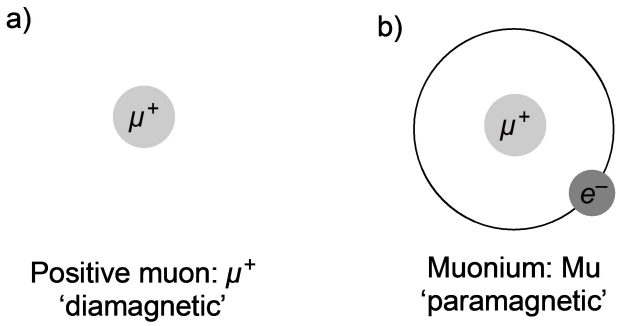

Figure 1. The nature of the final (positive) muon states of a) muon and b) muonium.

most cases, the hfc constants of the muoniation products are rather smaller compared with muonium itself.

The spin-polarized muons can be monitored by observing the muon's radioactive decay. When a muon decays, a positron e^+ and two neutrinos (ν) are emitted via the reaction of Equation (2). In this process, the positron is emitted preferentially along the direction of the muon spin at the moment of decay. Therefore, each muon decay gives rise to a positron whose direction contributes to a data point at a particular time *t*. By acquisition of millions of muon decay events (up to 10^8), it is possible to build up a histogram. The experiment data set is obtained as the collection of measured average spin polarization as a function of time after implantation.

$$\mu^+ \rightarrow e^+ + \nu_e + \bar{\nu}_\mu \quad (2)$$

The muonium has been useful for characterizing the radical addition reactions of organic compounds that are mostly difficult to observe by the ordinary chemical analysis. Muonium is formed by irradiation of a sample with muons, so there is no need for complicated mixtures necessary to produce H radical. The radicals are formed within 10 ns of implantation of the muon, which allows for the determination of the products formed solely by muonium addition. In the field of main group chemistry, West and Percival have demonstrated μSR studies for low-coordinated silicon compounds and the related group 14 element derivatives.[4] By using μSR, we have successfully characterized the radical reactions of several phosphorus heterocycles including unique unsaturated molecular structures. Besides the heterocycles, relevant low-coordinated phosphorus compounds have been studied by μSR. In this paper, the muoniation processes of the unsaturated phosphorus compounds are reviewed and discussed. Before that, some fundamentals of μSR techniques which will help understanding μSR are also described.

Shigekazu Ito was born in Iwate, Japan, in 1970. He received his PhD in 1998 from Tohoku University under the supervision of Prof. Masaaki Yoshifuji. After his postdoctoral stay in the group of Dr. Guy Bertrand (LCC–CNRS Toulouse, Université Paul Sabatier), he was employed as an assistant professor at Tohoku University in 1999. In 2008, he was appointed as an associate professor at Tokyo Institute of Technology. His current research interests include organophosphorus chemistry and muon science.

2. Fundamentals of μSR Experiments

In the application of μSR to organic compounds, transverse-field muon spin rotation (TF-μSR) and muon level-crossing resonance (μLCR) are frequently used. This section illustrates fundamentals of these two techniques concisely with reviewing the μSR studies of 1,3,5-tri-*t*-butylbenzene (Mes*H, **1**) and 2,4,6-tri-*t*-butylthiobenzaldehyde (Mes*CH═S, **2**). Both **1** and **2** are air-tolerant crystalline compounds, but it is possible to study air-sensitive compounds under the inert atmosphere conditions.

2.1. Transverse-field muon spin rotation (TF-μSR)

Figure 2a displays experimental set-up of a typical TF-μSR experiment. A magnetic field is applied to the sample in a direction perpendicular to the beam polarization. Muons are stopped in a sample and the elapsed time between individual

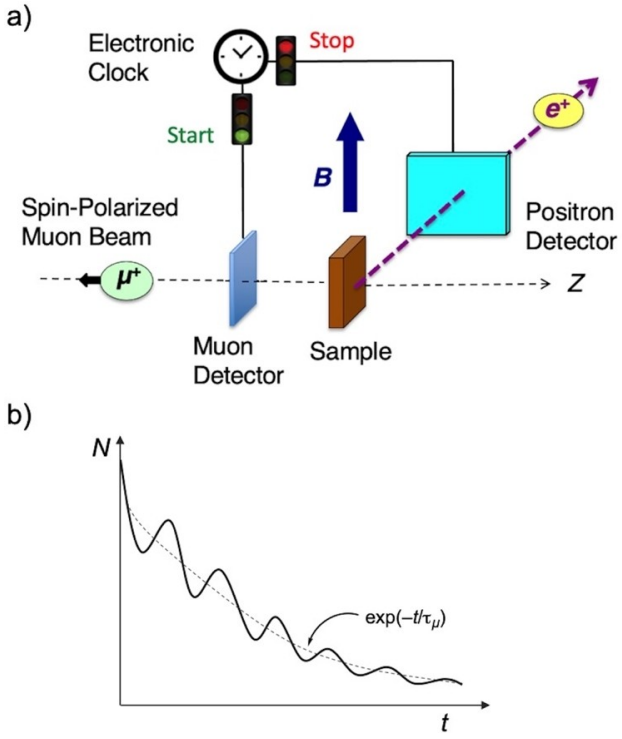

Figure 2. a) A schematic representation of the TF-μSR experiment. b) The elapsed time between the muon arrival and decay is recorded in a histogram. The average lifetime of muon is denoted as τ_μ.

muon stops and the detection of their decay positrons (see Eq 2) is recorded. Since the probability of detecting a decay positron in a particular direction depends on the orientation of the muon spin at the moment of its decay, the positron count oscillates in time as the muon spins past the detector. These oscillations are imposed on the lifetime histogram of the muon (Figure 2b). The time spectrum is Fourier transformed to display a frequency spectrum.

Muons in free radicals are subject to the local field of the unpaired electron – the hyperfine interaction. Figure 3 displays a Breit-Rabi diagram for isotropic muonium with a hyperfine constant appropriate for free (vacuum) muonium. At the high fields, only the 1↔2 and 3↔4 transitions can be observed. Accordingly, the muon precession frequency in a free radical can have two values (Eqs. (3) and (4)), corresponding to the two spin orientations of the unpaired electron:

$$\upsilon_{R1} = \nu_D - \frac{1}{2}A_\mu \quad (3)$$

$$\upsilon_{R2} = \nu_D + \frac{1}{2}A_\mu \quad (4)$$

where ν_D is the precession frequency of muons in diamagnetic environments, and the muon hyperfine coupling constant, A_μ is readily found from the difference of the two precession frequencies of the paramagnetic muoniums (radical signals ν_{R1} and ν_{R2}).

Figure 4 shows a TF-μSR spectrum of 1,3,5-tri-*t*-butylbenzene (Mes*H, **1**).[5] In this measurement, a 1.0 M solution of **1** in tetrahydrofuran (THF) was placed in a beam of positive muons from the TRIUMF cyclotron. The TF-μSR spectrum was collected at 298 K in a magnetic field of 1.45 T by using the Helios spectrometer. Muoniated radicals are characterized by a pair of precession frequencies, equally spaced about the diamagnetic signal (ν_D: 196 MHz in this case). The difference between the radical precession frequencies is equal to the muon hfc, A_μ. The hyperfine splitting constant is obtained by ν_{R2}-ν_{R1} [ν_{R2} (high): 430.2 MHz, ν_{R1} (low): −38.2 MHz], and the A_μ parameter of 468.4 MHz is comparable with cyclohexadienyl radical generated from muoniation of benzene (514.4 MHz). It is noteworthy that only one radical species is generated by the regioselective addition of muonium to **1**. The smaller intensity of the higher precession ν_{R2} correlates with the time resolution of the spectrometer.

Figure 5 displays a TF-μSR spectrum of crystalline 2,4,6-tri-*t*-butylthiobenzaldehyde (Mes*CH=S, **2**).[6,7] Similarly, the muoniated radicals are assigned by a characteristic pair of precession frequencies, equally spaced about the diamagnetic signal (ν_D: 136 MHz in this case). The hyperfine splitting constant is obtained by ν_{R2}–ν_{R1} [ν_{R2}: 164.7 MHz, ν_{R1}: 107.5 MHz], and A_μ of 57.2 MHz is determined, which enables to characterize the regioselective addition of muonium affording the carbon-

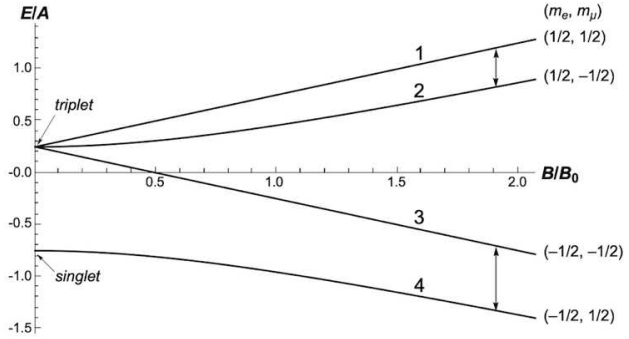

Figure 3. Sublevel energies of the Mu hyperfine interaction as a function of external magnetic field. Transitions 1↔2 and 3↔4 at the high field correlate with the precession frequencies of the radical signals ν_{R1} and ν_{R2}.

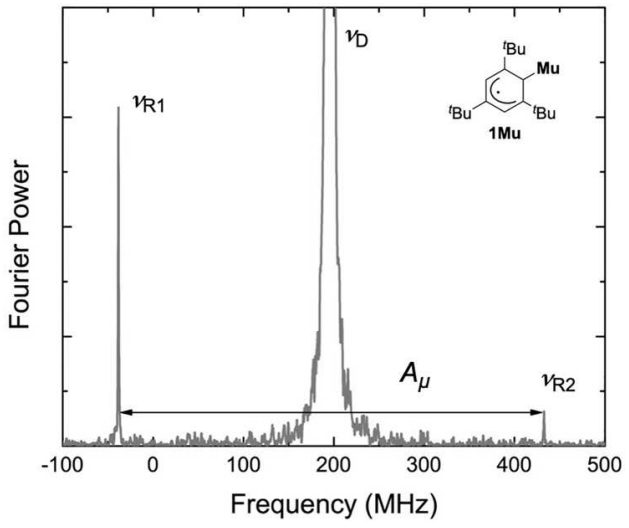

Figure 4. TF-μSR spectrum from a THF solution (1.0 M) of 1,3,5-tri-*t*-butylbenzene (Mes*H, **1**) at 298 K and 1.45 T. The ν_D peak is due to muons in diamagnetic molecules showing precession at the muon Larmor frequency. The hyperfine splitting constant A_μ is given by ν_{R2}–ν_{R1}. Adapted with permission from Ref. [5]. Copyright 2018, Wiley-VCH.

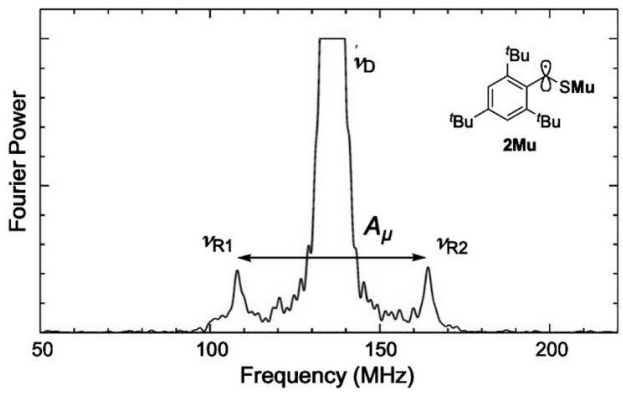

Figure 5. A TF-μSR spectrum of a powder sample of 2,4,6-tri-*t*-butylthiobenzaldehyde (Mes*CH=S, **2**) collected at 298 K in a magnetic field of 1.0 T. The sample was prepared as a pellet of 1–2 mm thickness covered with aluminum foil (11 μm thickness). Adapted with permission from Ref. [6]. Copyright 2019, Taylor & Francis.

centered radical species **2Mu**. The hyperfine splitting constant A_μ of **2Mu** is considerably smaller compared with the cyclohexadienyl radical, indicating that the muon hfc parameters are quite informative to characterize the structures of the muoniated paramagnetic species. It should also be mentioned that the aromatic group in **2** does not capture muonium, which is consistent with the rate constants for the reaction of muonium (k_M) with thioacetamide [MeC(=S)NH_2, $k_M = 3\times10^{10}$ $M^{-1}s^{-1}$)[8] and benzene ($k_M = 3.3\times10^9$ $M^{-1}s^{-1}$).[9] In addition, the 1-substituted 2,4,6-tri-*t*-butylphenyl group might be difficult to accept muonium due to the extreme steric congestion.

2.2. Muon level-crossing resonance (μLCR)

In muon *avoided* level-crossing resonance (μLCR) technique, the magnetic field is oriented parallel to the muon beam polarization, and the positron rate is measured in the forward and backward directions (Figure 6a). The difference in the rates is the muon asymmetry $A(t)$, which is proportional to the longitudinal muon spin polarization (Eq. (5)). N_F is the total number of positrons detected in the forward counters and N_B is the total number of positrons detected in the backward counters.

$$A(t) = \frac{N_B - N_F}{N_B + N_F} \tag{5}$$

For the coupled spin system of a muoniated free radical, there are some fields where mixing of a pair of spin states results in an avoided crossing. Therefore, μLCR technique is frequently described as avoided level-crossing muon spin resonance (ALC-μSR). If the mixed states involve different muon spin orientations, there is partial loss of spin polarization at the resonance field. In Figure 6b, M is the sum of the spin quantum numbers of the muon (μ), electron (e), and $I = 1/2$ nucleus (k).

For Δ_0 ($\Delta M = 0$) transitions, the resonant state involves an exchange between the muon spin and a nuclear spin. The level-crossing is avoided by indirect coupling of both Zeeman states to a third one. This avoided resonance occurs at a magnetic field according to Equation (6):

$$B_{res}^{\Delta_0} = \frac{1}{2}\left[\frac{A_\mu - A_k}{\gamma_\mu - \gamma_k} - \frac{A_\mu + A_k}{\gamma_e}\right] \tag{6}$$

where γ_μ, γ_k, and γ_e refer to the gyromagnetic ratios of the muon, nucleus of $I = 1/2$ spin, and electron, respectively. A_k is the hyperfine coupling constant of $I = 1/2$ nuclei.

Figure 7 shows a μLCR spectrum obtained from a 1.0 M solution of Mes*H (**1**) in THF at 298 K, obtained from the TRIUMF beamline with Helios spectrometer. The spectrum of differential-type line shape is due to field modulation. Since protons (^{1}H, p) are the only spin-active nuclei with large enough abundance to generate the spectrum, the resonance can be assigned to **1Mu**. The μLCR signal at 1.95 T and the A_μ constant, determined by the TF-μSR spectrum of Figure 4, gives the hyperfine coupling constant between the electron and proton

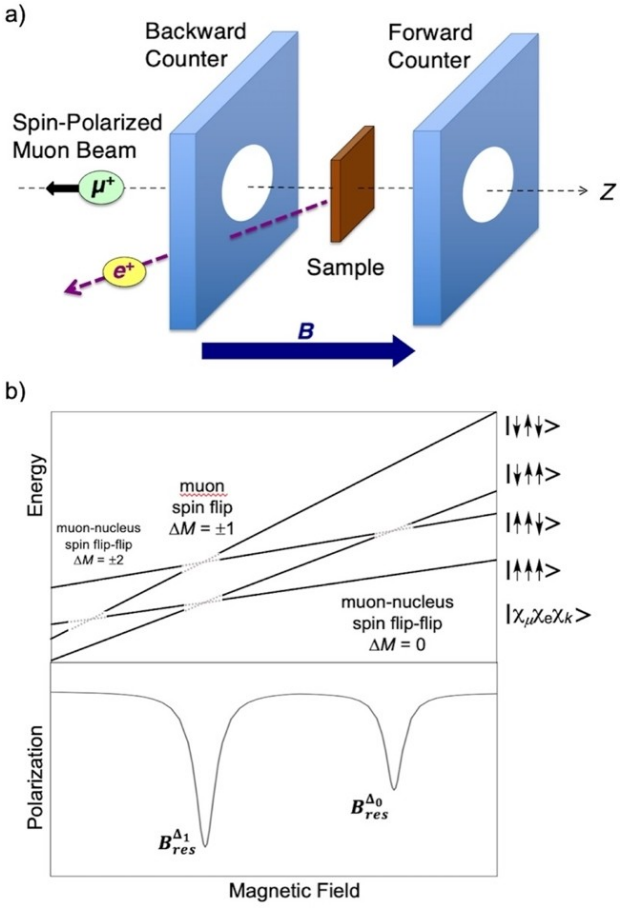

Figure 6. a) A schematic of μLCR experimental geometry. b) Top panel: Energy diagram for a three-spin system [muon (μ), electron (e), $I = 1/2$ nucleus (k)]. Bottom panel: LCR resonances occur when states with opposite muon spin become near-degenerate in energy. A transition with $\Delta M = \pm 2$, a muon-nucleus spin flip-flip transition, is usually very weak and rarely observed.

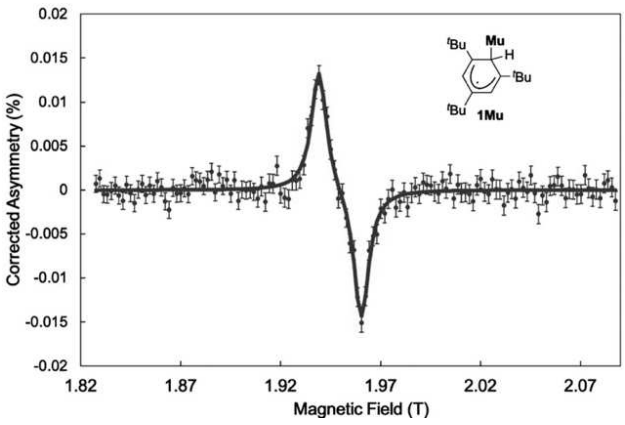

Figure 7. A μLCR spectrum of a 1.0 M THF solution of Mes*H at 298 K. Formula **1Mu** denotes the cyclohexadienyl radical generated by the regioselective addition of muonium to **1**. Only Δ_0 ($\Delta M = 0$) resonance was observed in the isotropic condition, and Δ_1 ($\Delta M = \pm 1$) resonance disappeared. Adapted with permission from Ref. [5]. Copyright 2018, Wiley-VCH.

(A_p) of 116 MHz.[5] The Δ_0 ($\Delta M = 0$) transitions are normally promoted by isotropic motion of the muoniated radicals.

The Δ_1 ($\Delta M = \pm 1$) transitions arise from mixing between spin states with the same electron and nuclear spins but different muon spin directions. These spin states are only mixed in the presence of anisotropy, and thus the Δ_1 resonance can be considered to be diagnostic of a frozen state or of anisotropic motion in such as crystalline and amorphous states. In this case, A_μ can be obtained according to Equation (7).

$$B_{res}^{\Delta_1} = \frac{1}{2}A_\mu\left[\frac{1}{\gamma_\mu} - \frac{1}{\gamma_e}\right] \quad (7)$$

Figure 8 shows a μLCR spectrum of **2** obtained by ARTEMIS spectrometer at the J-PARC synchrotron facility. The resonance at 0.21 T (2100 G) means 57.2 MHz of muon hfc, which is identical to the TF-μSR of **2Mu** (see Figure 5).

It is noteworthy that the Δ_1 ($\Delta M = \pm 1$) transition of **1Mu** is not observable in the solution, whereas a powder sample of **1** showed the μLCR signal at 1.71 T.[5]

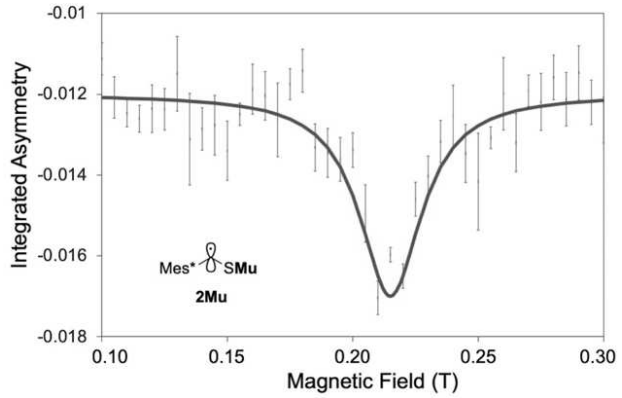

Figure 8. A μLCR spectrum of a powder sample of **2** at J-PARC equipped with ARTEMIS spectrometer. The resonance signal of **2Mu** was fitted with the Lorentzian curve. The sample was prepared as a pellet of 1–2 mm thickness covered with aluminum foil (11 μm thickness). Mes* = 2,4,6-tBu$_3$C$_6$H$_2$.

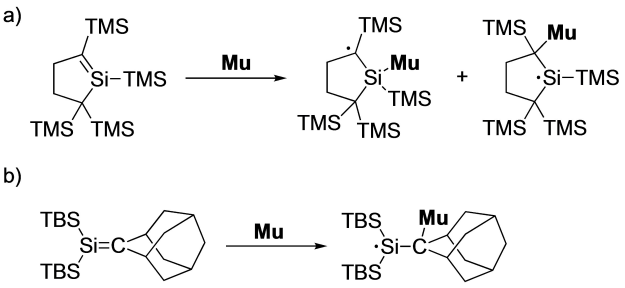

Figure 9. a) Muonium addition to a cyclic silene. TMS = $SiMe_3$. b) Muonium addition to a bulky *acyclic* silene. TBS = $SiMe_2{}^tBu$.

3. μSR Studies of Phosphorus Congeners of Acyclic Alkenes

The progress of main group chemistry has provided a number of isolable multiple bonds of heavier main group elements below the 2nd row. The heavier congeners of alkenes have been of interest from the views of radical reactivity with muonium. Silenes including Si=C double bonds can afford two muoniation (=addition of muonium) products via muonium processes at the C and Si atoms, and Figure 9a illustrates the example of a cyclic silene providing two muoniated radicals.[10] Steric bulkiness can control the regioselectivity, and Figure 9b displays single muoniation product.[4a]

Multiple bonds of phosphorus should be of interest for μSR studies. In this section, the recent studies on radical reactivity of a phosphaalkene and phosphasilenes are reviewed.

3.1. Muonium addition to an acyclic phosphaalkene

Phosphaalkenes are P=C analogs of alkenes and can be employed as monomers for radical polymerizations.[11] The discovery of an unexpected microstructure for the polymerized phosphaalkenes[12] suggested the importance of clarifying the free radical initiation step. In 2019, Gates and Percival and co-workers reported μSR studies for elucidating free radical reactivity of phosphaalkenes by using **3**.[13] Figure 10a displays muonium additions to **3** providing two radicals **3-PMu** and **3-CMu**. The muonium mainly generated **3-PMu** bearing the carbon-centered radical, and the muon hfc of 304 MHz was determined by TF-μSR. The minor P-centered radical **3-CMu** showed the smaller muon hfc (135 MHz) compared with **3-PMu**. Characterization of **3-PMu** and **3-CMu** was supported by using the alkene tautomer **4** which could afford the isotopologue of **3-PMu**, and the predominant formation of **4Mu** of $A_\mu = 254$ MHz was observed by TF-μSR (Figure 10b). It would be meaningful to mention that the Fourier transform signal intensity varies with respect to the muon arrival time. Although this behavior has

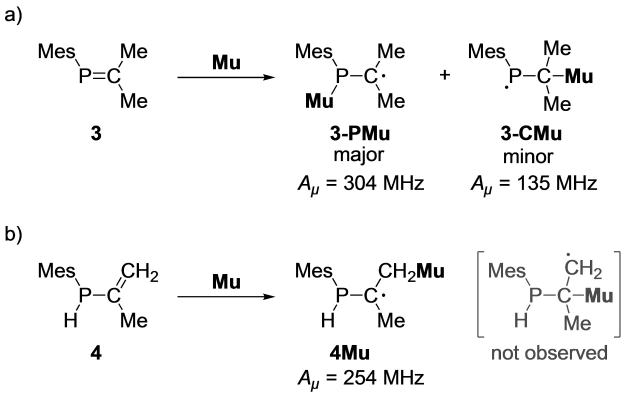

Figure 10. a) Muonium addition to phosphaalkene **3** affording **3-PMu** and **3-CMu**. Mes = mesityl (2,4,6-$Me_3C_6H_2$). b) Muonium addition to alkene **4** affording **4Mu**.

not been fully understood, it seems to indicate delayed formation of a radical.[4b] μLCR was employed for confirming the muonium radicals generated from **3** and **4**, because the Δ_0 ($\Delta M = 0$) transitions could determine hfcs of the $I = 1/2$ nuclei (^{31}P and ^{1}H). The assignment of ^{31}P hfc of **3-CMu** required checking temperature effects on μLCR spectra. Assigning the CH_3 and CH_2Mu proton nuclei was based on the temperature-dependent (CH_2Mu) and temperature-independent (CH_3) μLCR signals.[14] The resonance field positions and the corresponding ^{31}P and ^{1}H hfcs for **3-PMu**, **3-CMu**, and **4Mu** are shown in Table 2. It should be mentioned that the predicted muon hfc of ca. 230 MHz for **3-PMu** by scaling $A_p = 71.4$ MHz of P-*H* proton nucleus in **4Mu** with the ratio of magnetic moments of muon and proton (3.1833) is substantially smaller compared with the experimental A_μ of 304 MHz. This could be due to an isotope effect leading to increase of zero-point energies. The density functional theory (DFT) computations indicated that the Me-C–P-Mu dihedral angle in **3-PMu** changed by 4.6° compared with the Me-C–P-H in **4Mu**, whereas the vibrationally averaged P–Mu distance was slightly longer (1.4%).

3.2. Muonium addition to phosphasilenes

The heavier double bond units can be stabilized and isolable at the ambient temperatures by utilizing sterically demanding substituents and electronically perturbing units in synthesis. The Si=P double bond in phosphasilene is extremely reactive, but can be stabilized and isolated. Recently, Cai, Scheschkewitz, and Percival and co-workers reported synthesis and μSR study of silyl-substituted bulky phosphasilenes **5** (Figure 11a).[15] In this study, TF-μSR and intensive DFT calculations including potential energy surface (PES) scans were carried out.

The Mes- and Tipp-substituted phosphasilenes **5a** and **5b** gave only the Si-muoniation products **5a-SiMu** and **5b-SiMu**, whereas **5c** gave both **5c-PMu** and **5c-SiMu**. However, the non-detection of Si-centered radicals **5a-PMu** and **5b-PMu** does not completely rule out their formation, because the predicted muon hfc of 17 MHz is possibly swamped by the diamagnetic signal. Table 3 summarizes the assignments and conformations for muoniation of **5a–c** using dihedral angles θ_{Si} and θ_P that was determined by PES scans (Figure 11b). The single rotamer conformer of **5a-SiMu** was detected, and similarly the rotamers of P-centered radical **5c-SiMu** and Si-centered radical **5c-PMu** were observed. On the other hand, two rotamer conformations of **5b-SiMu** were characterized, suggesting that the presence of bulky Tipp group on the phosphorus was effective to define potential minima clearly. The two radicals **5b-SiMu**, obtained by the Fourier transform delay of 38 ns, indicate the substantially different energies, and correspondingly the TF-μSR paramagnetic signals of $A_\mu =$ 149 MHz were considerably small. In contrast to the expectation, muonium addition to **5d** gave at least four muoniated radicals. In all cases muonium addition to Si gives the lower energy radicals (**5-SiMu**). However, only the scans for **5d** include equiergic minima, indicating pairs of radical conformations with the same energy. Table 4 summarizes the assignments and conformations of **5d-SiMu** and **5d-PMu**.

Table 2. Analysis of μLCR spectra obtained from **3** and **4** in THF (0.5 M) at 25 °C.

Radical	Resonance field [kG]	Hyperfine constant [MHz]	Assignment[a]
3-PMu	5.986 ± 0.005	160.3 ± 0.2	*P*Mu
	13.173 ± 0.003	57.8 ± 0.1	$-C(CH_3)_2$
3-CMu	6.407 ± 0.008	285.1 ± 0.6	*P*–CMu
4Mu	4.779 ± 0.004	139.55 ± 0.09	*P*–H
	9.778 ± 0.004	71.40 ± 0.08	P–*H*
	10.481 ± 0.002	58.37 ± 0.04	CH_3
	10.772 ± 0.002	52.98 ± 0.04	CH_2Mu

[a] The nuclear spin is denoted by italic font.

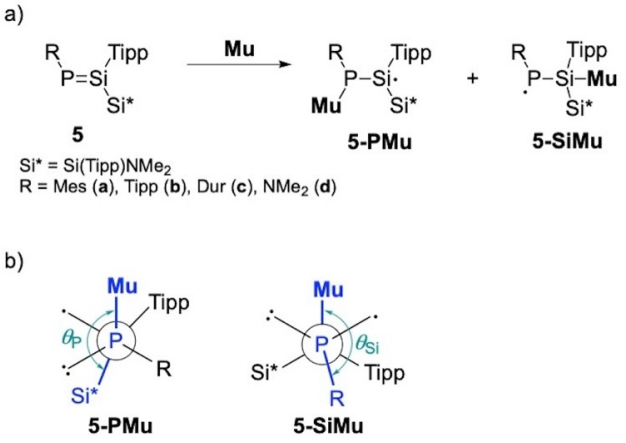

Figure 11. a) Muonium addition to sterically encumbered and electronically perturbed phosphasilenes **5**. Tipp = 2,4,6-iPr$_3$C$_6$H$_2$, Dur = 2,3,5,6-Me$_4$C$_6$H. b) Defining the dihedral angles θ_P and θ_{Si} for **5-PMu** and **5-SiMu**, respectively.

Table 3. Radical assignments and conformations generated from **5a–c**.

Radical[a]	Hyperfine constant [MHz] Expt.	Calcd.	Assignment Dihedral angle θSi or θP [°]	Energy[e] [kJ mol^{-1}]
5a-SiMu[b]	19	22	30	−248.8
5b-SiMu[c]	30	31	34	−251.6
	149	141	−66	−232.9
5c-SiMu[d]	21	21	30	−250.8
5c-PMu[d]	102	81	109	−226.6

[a] In THF (0.5 M). [b] At 53.5 °C. [c] At 53.7 °C. The two radicals were characterized by the Fourier transform delay of 38 ns. [d] At 54.6 °C. [e] Reaction energy, $DE = E$(radical) − E(parent) − E(H).

Table 4. Radical assignments and conformations generated from **5d**.

Radical[a]	Hyperfine constant [MHz] Expt.	Calcd.	Assignment Dihedral angle θ_{Si} or θ_P [°]	Energy[b] [kJ mol^{-1}]
5d-SiMu	46	43	213/−147	−242.7
	110	90	53	−241.6
5d-PMu	60	57	220/−140	−219.7
	20	19	320/−40	−219.7

[a] In THF (0.5 M), at 50.6 °C. [b] Reaction energy, $DE = E$(radical) − E(parent) − E(H).

Like the cases of phosphaalkene **3**, the μSR spectra were dependent on Fourier transform conditions, especially the time delay between the muon stop and the data time window used in the transform. The amplitudes of the precession frequencies vary with delay time in a sinusoidal manner. It should be noted that "standard" μSR display without Fourier transform delay can result in missing a particular signal. Whereas the spectrum derived from **5b** revealed two radicals (see Table 3), adjustment of the transform delay time to 53 ns revealed the (uncharacterized) precession signals of a third radical of hfc = 62 MHz.

4. μSR Studies of a *peri*-Trifluoromethyl-Substituted 9-Phosphaanthracene

Anthracene is a typical condensed aromatic hydrocarbon showing several functional physical properties, and its radical reactivity is of interest from the views of bioactivity, combustion affording polyaromatic hydrocarbons, and oxidation in relation to environment science.[16] Attempts to exchange the skeletal sp^2 carbon atom with the heavier p-block elements have been performed because, for example, the small bandgap of the heavier double bonds would realize novel functional π-conjugated heterocyclic systems. 9-Phosphaanthracene is one of the heavier congeners of anthracene. Whereas most of the 1,8-non-substituted 9-phosphaanthracenes are labile, use of the trifluoromethyl (CF_3) groups as the *peri* (1,8-positions) substituents is a promising method to synthesize air-tolerant 10-aryl-9-phosphaanthracenes.[17]

We employed 10-mesityl-1,8-bis(trifluoromethyl)-9-phosphaanthracene (**6**) for the μSR study (Figure 12).[18] Figure 12a displays a TF-μSR spectrum of a THF solution (0.16 M) of **6** at 298 K. A transverse magnetic field of 1.45 T corresponds to the diamagnetic signal (ν_D) of 196 MHz, and the difference between the radical precession frequencies (ν_{R2}-ν_{R1}) is equal to the absolute muon hfc (A_μ) of 221.83 ± 0.04 MHz. This TF-μSR spectrum is compatible with the regioselective addition of muonium to **6** affording single observable radical species, which is in sharp contrast to the muoniation of anthracene affording three (or four) paramagnetic species.[19] Taking the potent high reactivity of P=C into account (see μSR of **3** in Section 3.1),[13] muonium would predominantly add to the phosphorus atom, and the benzene rings are reluctant to accept muonium. To confirm the regioselective muoniation, we conducted μLCR experiments with an isotropic solution sample of **6**. As shown in Figure 6b and Equation (6), the nucleus hyperfine constant (A_k) of a half-integer nuclear spin ($I = 1/2$) can be determined by using the Δ_0 avoided level-crossing resonance magnetic field and muon hyperfine constant (A_μ). A μLCR spectrum obtained from a THF solution of **6** at 298 K is displayed in Figure 12b. The highly plausible regioselective addition of muonium at the phosphorus atom in **6** means that the observable spin-active $I = 1/2$ nucleus would be only ^{31}P with large enough abundance to generate the spectrum. The avoided level-crossing resonance magnetic field at 5.18 kG and

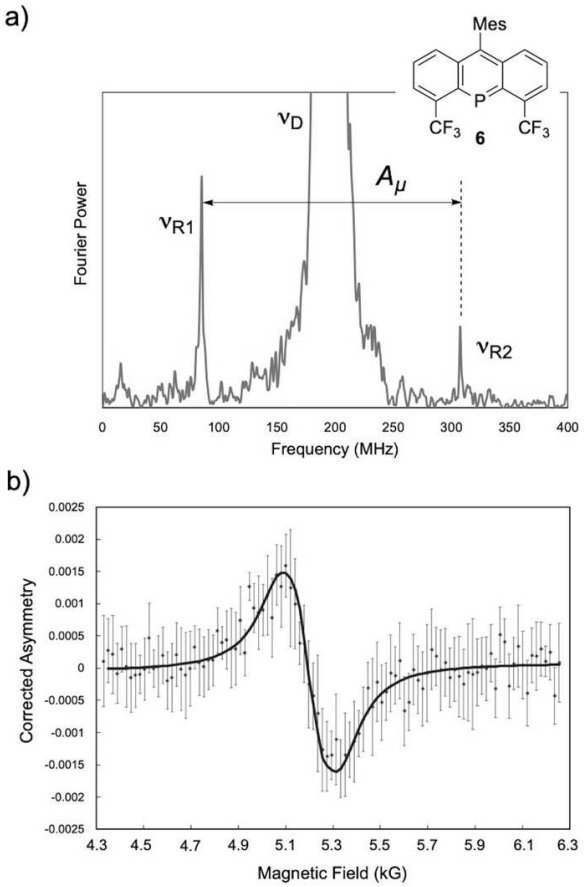

Figure 12. a) TF-μSR spectrum of 9-phosphaanthracene **6** (THF solution, 0.16 M) at 298 K and field of 1.45 T. $A_\mu = 221.83 \pm 0.04$ MHz. Mes = mesityl (2,4,6-$Me_3C_6H_2$). b) A μLCR spectrum of a 0.16 M solution of **6** in THF at 298 K. The resonance at 5.18 kG can be assigned as hfc of ^{31}P nucleus (98.0 ± 1.1 MHz). The differential-type line-shape is due to the field modulation. Adapted with permission from Ref. [18]. Copyright 2021, Wiley-VCH.

the A_μ parameter determined by the TF-μSR spectrum in Figure 12a provides the hyperfine coupling constant of ^{31}P nucleus [$A_k(^{31}P)$] as 98.0 ± 1.1 MHz. In combination with the TF-μSR experiment, the μLCR data strongly suggested that the muonium added to the phosphorus in **6**.

The TF-μSR and μLCR results of **6** are compatible with the regioselective addition of muonium to the phosphorus atom providing **6Mu** (Figure 13a), and structure characterization was the subsequent task. In the DFT calculations, the H atom was employed in the place of Mu, and the muon hfc was calculated by multiplying the relative gyromagnetic ratio to proton ($\gamma_\mu/\gamma_p = 3.1833$). The ordinary DFT structure optimization at the UωB97XD/6-311G(d,p) level, where Mu was calculated as H atom in optimizing the structures, provided the structure showing remarkable envelope-type conformation of the 6-membered phosphorus heterocycle (Figure 13b).[18] The notable butterfly-like tricyclic skeleton is promoted by both the P–Mu unit and the flanking CF_3 group. However, the A_μ^{calc} of the optimized structure is considerably smaller (107 MHz) compared with the experimentally determined A_μ (222 MHz), suggesting

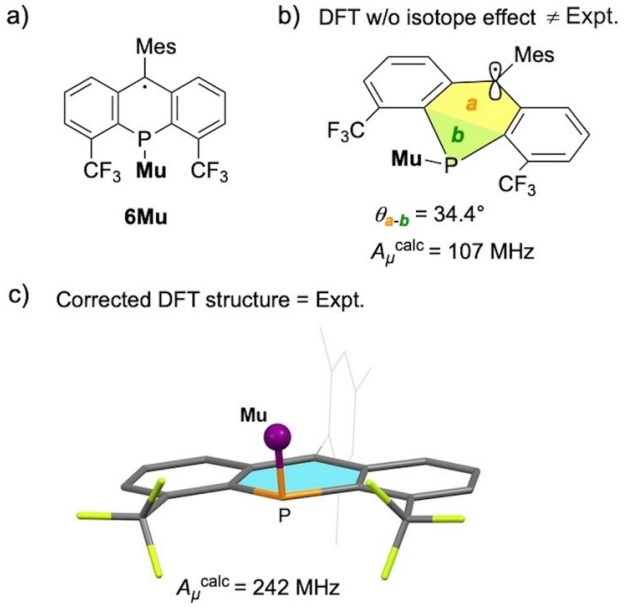

Figure 13. a) Formula of the muoniated radical **6Mu**. b) A description for the normally DFT-optimized structure of **6Mu** under the conditions of UwB97XD/6-311G(d,p). The P-containing 6-membered ring is butterfly-like, and the calculated muon hfc is not consistent with the experimental data of Figure 12a. c) A plot of the corrected DFT structure of **6Mu** at the UωB97XD/6-311G(d,p) level. The phosphorus-containing 6-membered ring, colored in light blue, is almost flat, and the three-cyclic skeleton is nearly planar.

that the light mass of Mu accompanying larger zero-point energy avoids formation of the theoretically most stable conformer. In the muoniation to cyclic molecules, the isotope effect could be normally characterized by elongation of the X–Mu bond, where X is C atom or other main group elements, due to higher zero-point vibration promoting increase of the average bond distance.[1,3,5,20] However, both elongation of the P–Mu(H) bond and scanning the angles around the phosphorus based on the rocking and wagging motions could not simulate the experimental muon hfc. After many calculation trials, we attempted modification of the butterfly-like tricyclic skeleton of the normal DFT structure by considering the "concave" form of the phosphorus heterocycle. Fortunately, the corrected structure shown in Figure 13c provided the estimated muon hfc of 242 MHz which was comparable with the experimentally determined A_μ (222 MHz). The tricyclic skeleton of **6Mu** in Figure 13c is almost planar, and the sum of the internal bond angles of the P-containing heterocycle is up to 723.6°. Whereas the calculated ^{31}P hfc for Figure 13c (74.4 MHz) was deviated from the experimental hfc [$A_k(^{31}P) = 98$ MHz], modifying the structure by increasing the pyramidalization around the phosphorus atom could produce a ^{31}P hfc of 96.4 MHz close to the experimental $A_k(^{31}P)$. The successfully characterized isotope effect causing the remarkable motion of the molecular skeleton in **6Mu** would be promoted by the flexible fused heavier heterocyclic system and the fluorine-containing substituents.

Furthermore, TF-μSR measurements using a powder sample of **6** were attempted, and resulted in determining the absolute A_μ of 254.7 ± 0.6 MHz.[18] The substantially different A_μ parameters between the solution and the powder samples (ΔA_μ = 33 MHz) would not be comparable with the A_μ data of the exohedral muonium adduct on C_{60} (ΔA_μ = 6.5 MHz).[21] However, the deviation of ΔA_μ = 33 MHz is comparable with the temperature A_μ dependence of such as cyclohexadienyl radicals on SiO_2 surface[22] and the paramagnetic species in clathrate hydrate of 2,5-dihydrofuran.[23] Thus, the TF-μSR spectrum of **6** indicates effects of the environment promoting scalable structural change of the muoniation product of **6** due to the flexibility of the heavier anthracene-type framework. Also, the solid sample of **6** was applicable to μLCR measurements, and Figure 14 displays a μLCR spectrum of **6** in the solid state. The weak Δ_0 resonance at 0.51 T is compatible with the hfc of ^{31}P nucleus in **6Mu** (see Figure 12b). The Δ_1 resonance at 0.93 T means muon hfc (254 MHz) of **6Mu**, which is compatible with the TF-μSR result described above. Correspondingly, the ^{31}P hfc [$A_k(^{31}P)$] would be 132 MHz in the solid state, indicating the deviation from that of the solution up to 34 MHz. The observation of both Δ_0 and Δ_1 of **6Mu** should correlate with the solid state properties of **6**.[3a,b,24] Another Δ_1 resonance at 1.78 T would be a small amount of the paramagnetic species via muoniation to the *meso*-substituted mesityl group in **6**, because the muon hfc of 486 MHz is typical of a cyclohexadienyl radical derived from a benzene derivative. The minor muoniation could be observed by μLCR which enables experiments with small amount (low concentration) of precursor molecule.[3a]

5. μSR Studies of 1,3-Diphosphacyclobutane-2,4-diyl (BR)

A cyclobutane-1,3-diyl is the most fundamental cyclic organic biradical species and is normally observable only under cryogenic conditions because of its instability. However, exchange of the skeletal elements in the cyclobutane-1,3-diyl with the hetero-elements is an effective approach to reduce the

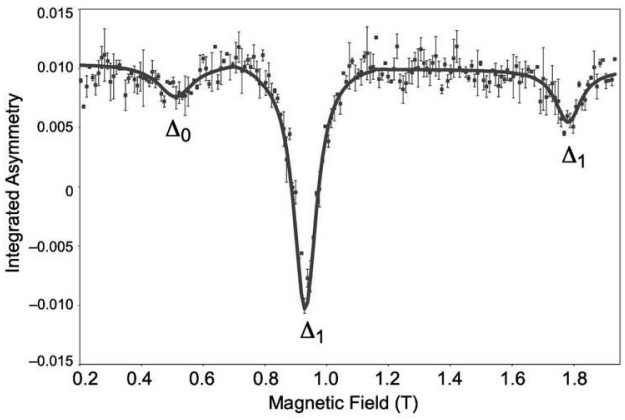

Figure 14. A μLCR spectrum of a powder sample of **6** at 298 K. The Δ_0 resonance at 0.51 T is compatible with the hfc of ^{31}P nucleus in **6Mu**. The Δ_1 resonance at 0.93 T is compatible with the muon hfc of **6Mu**. The Δ_1 resonance at 1.78 T would correlate with *minor* muoniation to the *meso*-mesityl group in **6**.

open-shell character. A sterically encumbered 1,3-diphosphacyclobutane-2,4-diyl (Figure 15a) is one of such heavier congeners of cyclobutane-1,3-diyl.[25,26] Our intensive studies have been successful in developing highly air-stable 1,3-diphosphacyclobutane-2,4-diyls (hereafter abbreviated as **BR**s), which have opened new avenues for applications.[27] Several air-tolerant **BR**s work as good electron-donors, and also are useful to fabricate low-voltage p-channel transistors.[28] Also, the presence of tervalent phosphorus atoms enables to afford particular phosphorus heterocycles via valence expansion, and until now formal capture of dihydrogen[29] and sensing of hydrogen fluoride[28b,30] have been developed. These functional aspects of air-tolerant **BR**s should be promoted by the presence of particular biradicalic electrons, which can be assessed by chemical processes including radical additions. However, observation of paramagnetic species by radical addition to **BR** has been quite difficult. For example, we tentatively observed a regioselective interaction of **BR** with O_2, which might be promoted by the strength of P–O linkage and the zwitterionic canonical formula (Figure 15b). It has been unsuccessful to obtain appropriate samples of the O_2 adduct for completion of the structural analysis.

In the course of our studies on the particular phosphorus heterocycle of biradicalic structure, we thought that one of the effective approaches for investigating radical reactivity of the sterically encumbered **BR** would be muon spectroscopy. Several advantages using muonium enabled characterization of the regioselective radical addition to N-heterocyclic carbene (NHC).[31] Also, it should be mentioned that West and Percival and co-workers demonstrated use of muonium for characterizing radical reactions of the silicon analog of NHC.[4,32] Although it is likely that the presence of aromatic substituents is undesirable for the probing with muon because benzene can capture muonium, the result of West and Percival that a sterically encumbered silylene bearing the 2,6-diisopropylphenyl groups provided the corresponding radical via regioselective muonium addition to the silicon centre[32a] stimulated to utilize μSR for studies of **BR**s displayed in Figure 15a.

5.1. Muoniation at the P atom

Figure 16 illustrates the results of μSR for the bulky **BR** bearing *t*-butyl and benzyl substituents on the phosphorus atoms (**7**).[5] Compound **7** is functional as a p-type organic field-effect transistor (OFET) working with considerably small gate voltages.[28a,c] We first attempted TF-μSR experiments with **7**, but unfortunately a THF solution sample gave no clear information about muon hyperfine parameters. So, we decided to conduct μLCR spectroscopy with a powder sample of **7**. As mentioned above, the radical in crystals and solids is undergoing anisotropic motion or slow isotropic reorientation, and can show the avoided level-crossing resonance due to only spin-flip of muon ($\Delta M = \pm 1$, Figure 6b). As we expected, the resonance due to the $\Delta M = \pm 1$ transition of radical species generated from **7** was observed in the range of 0.18–0.20 T (Figure 16a). No resonance was observed in the spectrum of Mes*H (**1**) in the same range, indicating that the alkyl-substituted aryl substituents as well as benzyl group were not responsible to provide the resonance

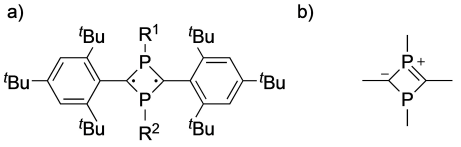

Figure 15. a) Chemical formula of the air-tolerant 1,3-diphosphacyclobutane-2,4-diyl (**BR**). b) A zwitterionic canonical formula of **BR**.

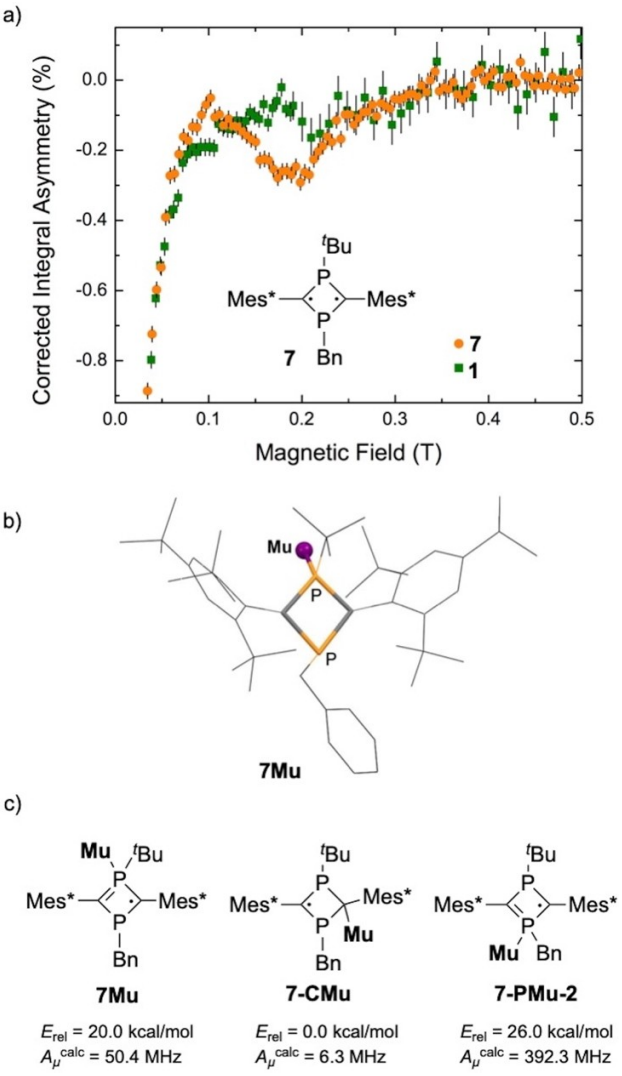

Figure 16. a) μLCR spectra of powder samples of **7** (orange circles) and **1** (Mes*H, green squares) at 298 K. Field modulation is not employed. The resonance in the range of 0.18–0.20 T corresponds A_μ of 46.2 ± 0.3 MHz. Bn = benzyl (CH_2Ph). Mes* = 2,4,6-*t*$Bu_3C_6H_2$. b) The DFT-optimized structure of **7Mu** showing the calculated muon hfc of 50.4 MHz [UrevPBE-D3(BJ)/TZ2P-J//UBP86-D/TZ2P]. c) Possible isomers generated by muonium addition to **7**. The structures were optimized at the UBP86-D/TZ2P (ZORA = scaler), and the total energies were calculated under the condition of ZORA = none. Absolute muon hfc was obtained at the UrevPBE-D3(BJ)/TZ2P-J level. The isotope effect is not considered. Adapted with permission from Ref. [5]. Copyright 2018, Wiley-VCH.

signal of 0.18–0.20 T. According to Equation (7), the A_μ constant of 46.2 ± 0.3 MHz is determined for the muonium radical produced from **7**. The radical observed in μLCR spectroscopy of **7** was characterized by the DFT calculations. Figure 16b displays the assigned structure **7Mu**, where the muonium adds to the *t*Bu-substituted phosphorus atom showing the calculated muon hfc of 50.2 MHz at the UrevPBE-D3(BJ)/TZ2P-J//UBP86-D/TZ2P level.[5] It should be considered that the light mass of muonium promotes higher zero-point energies than hydrogen leading to significant isotope effects from conformational averaging. According to the preliminary studies using the truncated P-heterocyclic molecular structure, the light isotope effect could appear as 4% extension of P–Mu distance compared with P–H. The light isotope effect causes increase of the calculated muon hfc to 59.7 MHz, indicating the deviation from the experimentally determined A_μ is still compatible with the structural characterization. The difference between the experimental data and the computational result might be reduced by improving the DFT conditions. For example, the absolute muon hfc of 44.3 MHz was estimated for **7Mu** [including 4% P–Mu(H) extension] at the UB3LYP/6-311G(d,p)//UM06-2X/6-31G(d) level. The *t*BuP-selective addition of *nucleophilic* muonium[33,34] to the sterically encumbered but positively charged phosphorus atom in **7** might be comparable with the regioselective addition of hydride of $LiAlH_4$[29] and fluoride ion[30] to **BR**s.

Figure 16c shows the possible muoniations of **7**. It is obvious that addition of muonium to the skeletal radicalic carbon providing **7-CMu** (*trans* isomer) is thermodynamically preferable. The muoniation at the benzyl-substituted phosphorus atom leading to **7-PMu-2** shows the considerably large deviation of muon hfc from the experimental result. One of the reasons why addition of muonium to the *t*Bu-substituted phosphorus atom was predominantly observed would be explained by the small activation energy compared with the C-muoniation. In this case, the activation energy was roughly estimated according to the trajectory of P–Mu(H) bond of the DFT-optimized structure. The finding that only μLCR enabled to observe **7Mu** would correlate with the small amount of the muoniation process[3a] probably because of the energetically less favorable structure bearing the $\lambda^5\sigma^4$-phosphorus atom.

It should be mentioned that crystalline samples of air-tolerant **8** which did not show the transistor behavior gave no observable muoniation species. Figure 17 displays the crystal structures of **7** and **8**.[28c] Compound **7** constructs the effective hole transfer pathways. On the other hand, **8** contains the dimers showing the small hole couplings of 0.07 and 0.05 meV. Although detailed studies are required, the crystal structure of **BR** might correlate with the reactivity toward muonium.

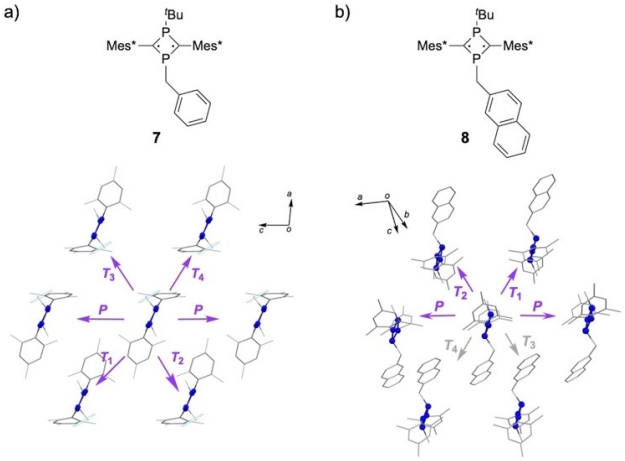

Figure 17. a) Crystal structure of **7** in the monoclinic space group. All dimers (*P*, T_1-T_4) showed the hole couplings of 0.69 meV or more [PW91/TZ2P]. The methyl groups and hydrogen atoms are omitted. Mes* = 2,4,6-tBu$_3$C$_6$H$_2$. b) Crystal structure of **8** in the triclinic space group. Dimers T_3 and T_4 showed the hole couplings of 0.07 and 0.05 meV, respectively. Adapted with permission from Ref. [28c]. Copyright 2016, Wiley-VCH.

5.2. Muoniation at the radicalic C atom

As described above, the observed radical **7Mu** meant addition of muonium to the phosphorus atom bearing the *t*Bu group in **7**. Probably due to the less steric hindrance, the muoniation process to the *t*Bu-substituted phosphorus in **7** might be controlled kinetically. However, addition of muonium to the skeletal C atom in **BR** is thermodynamically favorable and cannot be excluded. It is noteworthy that one of the N,P-heterocyclic congeners of cyclobutane-1,3-diyl, namely [·P(μ-NTer)$_2$P·], can accept Et· radical at the radicalic P centre.[35] As described below, our recent μSR experiments succeeded in finding the C-muoniation of **BR**.[36]

In the series of μSR experiments for **BR**, we worked with a powder sample of 2,4-bis-(2,4,6-tri-*t*-butylphenyl)-1-*t*-butyl-3-(3,5-dichloro-2,4,6-triazinyl)-1,3-diphosphacyclobutane-2,4-diyl (**9**).[28a] The electron-deficient N-heterocyclic substituent in **9** reduces the *HOMO-LUMO* gap, probably enabling easier access to the triplet state. The muon beamline at the TRIUMF cyclotron was used, and the LAMPF spectrometer was equipped. Figure 18a displays a TF-μSR spectrum collected at 298 K in a transverse magnetic field of 2 kG. Muonium radicals are characterized by a characteristic pair of precession frequencies, equally spaced about the diamagnetic signal of $\nu_D = 27.2$ MHz in this case. The larger muon hfc of 6.5 MHz is obtained by ν_{R2a} and ν_{R1a}, and similarly the smaller muon hfc of 4.5 MHz can be determined from ν_{R2b} and ν_{R1b}. These muon hfc parameters determined by the TF-μSR measurement of **9** are remarkably smaller compared with **7Mu**, indicating that muonium avoids interacting with the *t*-butylated phosphorus atom in **9**. In addition, the experimentally determined muon hyperfine parameters indicate that the aryl units in **9** do not capture muonium. It was possible to conclude that muonium added to the radicalic skeletal carbon atoms in **9** affording paramagnetic **9Mu** as a mixture of *trans* and *cis* isomers (Figure 18b). Almost no deviation of the theoretical muon hfc constants was characterized even by elongation of the C–Mu(H) distances due to the possible light isotope effect. The muoniation processes toward the skeletal phosphorus atoms in **9** were also examined by DFT calculations, and one of the P-muoniation products showed similar muon hyperfine parameter to *trans*-**9Mu**.

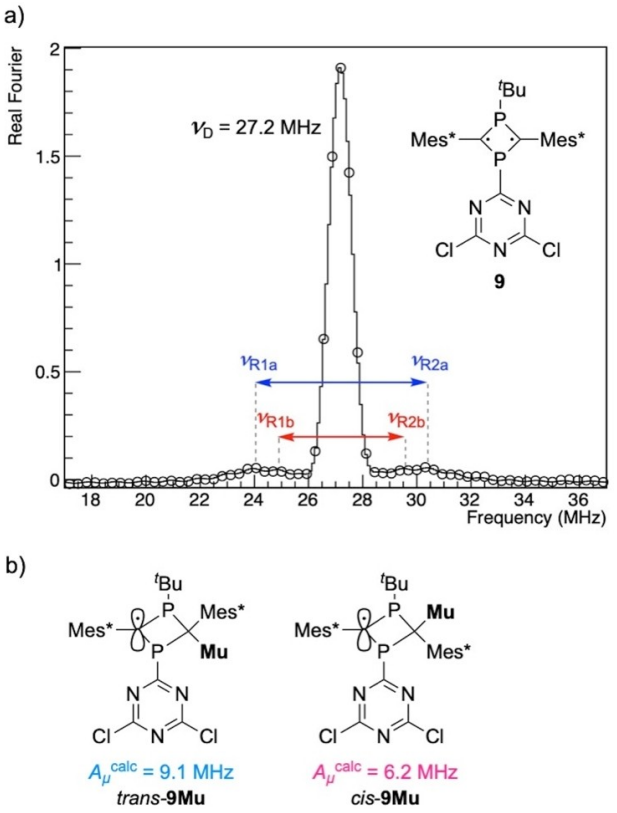

Figure 18. a) TF-μSR spectrum from a powder sample of **9** at 298 K and field of 2 kG. A strong diamagnetic resonance of muon (ν_D) appears at 27.2 MHz. Two muon hfcs [6.5 MHz (ν_{R2a}–ν_{R1a}, blue) and 4.5 MHz (ν_{R2b}–ν_{R1b}, red)] are characterized. b) Formulas of the muoniated species generated from **9**. The calculated muon hfc parameters (absolute) are obtained at the UPBE-MBD@rsSC/TZ2P-J//UwB97XD/6-311G(d,p) level. Mes* = 2,4,6-tBu$_3$C$_6$H$_2$. Adapted with permission from Ref. [36]. Copyright 2021, The Chemical Society of Japan.

However, the relative total energy is considerably high, probably because the chlorinated N-heterocyclic group largely destabilizes the positively charged $\lambda^5\sigma^4$ phosphorus unit. Furthermore, the pair of two radicals by muoniation of **9** suggests the presence of geometrical isomers, which is compatible with two radical species *trans*-**9Mu** and *cis*-**9Mu**. The C-selective addition of muonium to **9** providing **9Mu** might correlate with the structural aspects of the reduced singlet-triplet energetic difference and the increased open-shell characters of the skeletal carbons.

6. Conclusion and Outlook

This paper has described fundamentals of μSR for studying radical reactions with muonium of light hydrogen surrogate, and has summarized recent μSR studies for elucidating the radical reactions of organophosphorus compounds including the unsaturated structures. Phosphaalkene **3** and phosphasilenes **5** showed the predominant muonium addition to the P=C and P=Si units, and the corresponding radicals have been characterized by considering the isotope effect and the conformational properties. The 9-phosphaanthracene which are trifluromethylated at the *peri* positions (**6**) showed the regioselective addition of muonium leading to the single paramagnetic species, and the organofluorine groups were responsible to promote the unprecedented isotope effect leading to the planar three-cyclic molecular unit. 1,3-Diphosphacyclobutane-2,4-diyls (**BR**s) **7** and **9** showed the predominant capture of the muoniums at the phosphorus and the carbon in the 4-membered phosphorus heterocycle providing **7Mu** and two geometrical isomers of **9Mu**. These regioselective muoniations would correlate with the zwitterionic canonical structure and the open-shell character of the P_2C_2 cyclic unit as well as the steric effect.

It is possible to confirm the usefulness of muon from accelerators for intensive studies on organic radical reactions. The μSR studies on the unsaturated phosphorus molecules have clarified that radical additions occur at the heavier double bonds and open-shell singlet heterocycle with the high regioselectivity. In the muoniation process, the light isotope effect causing unique molecular motions providing the higher-energy paramagnetic species should be considered. Uncovered physical phenomena caused by the light surrogate of proton and hydrogen will exist and be fruitful to explore novel paramagnetic molecular functionality produced by main group chemistry.

Acknowledgements

The author thanks Dr. Iain McKenzie and Dr. Kenji M. Kojima of Centre for Molecular and Materials Science (CMMS) at TRIUMF (Experiments M1497, M1800), Prof. Koichi Mikami, Dr. Yasuhiro Ueta, Kota Koshino, Naoto Kato, and Hikaru Akama of Tokyo Institute of Technology. The staff of CMMS at TRIUMF supported the TF-μSR and μLCR measurements. Dr. Kerim Samedov, Henry T. G. Walsgrove, and Prof. Derek P. Gates of The University of British Columbia supported preparations of the μSR samples. Prof. Akihiro Koda, Dr. Shoichiro Nishimura, and Dr. Jumpei Nakamura of KEK-IMSS (High Energy Accelerator Research Organization, KEK - Institute of Materials Structure Science) supported the μSR experiments at J-PARC (Experiment 2020 A0019). The author thanks Prof. Toshiyuki Takayanagi of Saitama University and Masanori Tachikawa of Yokohama City University for discussing about theoretical calculations. The μSR works were supported in part by Grants-in-Aid for Scientific Research (No. 19H02685) from the Ministry of Education, Culture, Sports, Science and Technology, the Collaborative Research Program of Institute for Chemical Research, Kyoto University, and by grants from Yamaguchi Educational and Scholarship Foundation, Foundation for High Energy Accelerator Science, and Harmonic Ito Foundation. Nissan Chemical Industries Ltd. supported financially.

Conflict of Interest

The authors declare no conflict of interest.

Data Availability Statement

Research data are not shared.

Keywords: isotope effect · muon · muonium · phosphorus · radicals

[1] S. J. Blundell, R. de Renzi, T. Lancaster, F. L. Pratt, Eds., *Muon Spectroscopy – An Introduction* Oxford University Press, Oxford, **2022**.

[2] a) K. Nagamine, *Introductory Muon Science* Cambridge University Press, **2003**; b) E. Roduner, *The Positive Muon as a Probe in Free Radical Chemistry (Lecture Notes in Chemistry 49)*, Springer, Berlin, **1988**; c) D. C. Walker, *Muon and Muonium Chemistry* Cambridge University Press, **1983**.

[3] a) I. McKenzie, *Annu. Rep. Prog. Chem. Sect C: Phys. Chem.* **2013**, *109*, 65–112; b) I. McKenzie, E. Roduner, *Naturwissenschaften* **2009**, *96*, 873–887; c) S. J. Blundell, *Chem. Rev.* **2004**, *104*, 5717–5736; d) C. J. Rhodes, *J. Chem. Soc. Perkin Trans. 2* **2002**, 1379–1396; e) E. Roduner, *Chem. Soc. Rev.* **1993**, *22*, 337–346.

[4] a) R. West, K. Samedov, P. W. Percival, *Chem. Eur. J.* **2014**, *20*, 9184–9190; b) R. West, P. W. Percival, *Dalton Trans.* **2010**, *39*, 9209–9216.

[5] S. Ito, Y. Ueta, K. Koshino, K. M. Kojima, I. McKenzie, K. Mikami, *Angew. Chem. Int. Ed.* **2018**, *57*, 8608–8613; *Angew. Chem.* **2018**, *130*, 8744–8749.

[6] S. Ito, N. Kato, Y. Ueta, K. Mikami, K. M. Kojima, *Phosphorus Sulfur Silicon Relat. Elem.* **2019**, *194*, 735–738.

[7] a) R. Okazaki, A. Ishii, N. Fukuda, H. Oyama, N. Inamoto, *J. Chem. Soc. Chem. Commun.* **1982**, 1187–1188; b) A. Ishii, T. Ishida, N. Kumon, N. Fukuda, H. Oyama, N. Inamoto, F. Iwasaki, R. Okazaki, *Bull. Chem. Soc. Jpn.* **1996**, *69*, 709–717.

[8] M. V. Barnabas, K. Venkateswaran, D. C. Walker, *Can. J. Chem.* **1989**, *67*, 120–126.

[9] J. M. Stadlbauer, B. W. Ng, R. Ganti, D. C. Walker, *J. Am. Chem. Soc.* **1984**, *106*, 3151–3153.

[10] B. M. McCollum, T. Abe, J.-C. Brodovitch, J. A. C. Clyburne, T. Iwamoto, M. Kira, P. W. Percival, R. West, *Angew. Chem. Int. Ed.* **2008**, *47*, 9772–9774; *Angew. Chem.* **2008**, *120*, 9918–9920.

[11] a) C.-W. Tsang, M. Yam, D. P. Gates, *J. Am. Chem. Soc.* **2003**, *125*, 1480–1481; b) C.-W. Tsang, B. Baharloo, D. Riendl, M. Yam, D. P. Gates, *Angew. Chem. Int. Ed.* **2004**, *43*, 5682–5685; *Angew. Chem.* **2004**, *116*, 5800–5803.

[12] a) P. W. Siu, S. C. Serin, I. Krummenacher, T. W. Hey, D. P. Gates, *Angew. Chem. Int. Ed.* **2013**, *52*, 6967–6970; *Angew. Chem.* **2013**, *125*, 7105–7108; b) B. W. Rawe, A. M. Priegert, S. Wang, C. Schiller, S. Gerke, D. P. Gates, *Macromolecules* **2018**, *51*, 2621–2629.

[13] L. Chandrasena, K. Samedov, I. McKenzie, M. Mozafari, R. West, D. P. Gates, P. W. Percival, *Angew. Chem. Int. Ed.* **2019**, *58*, 297–301; *Angew. Chem.* **2019**, *131*, 303–307.

[14] P. W. Percival, J.-C. Brodovitch, S.-K. Leung, D. Yu, R. F. Kiefl, G. M. Luke, K. Venkateswaran, S. F. J. Cox, *Chem. Phys.* **1988**, *127*, 137–147.

[15] K. Samedov, Y. Heider, Y. Cai, P. Willmers, D. Mühlhausen, V. Huch, R. West, D. Scheschkewitz, P. W. Percival, *Angew. Chem. Int. Ed.* **2020**, *59*, 16007–16012; *Angew. Chem.* **2020**, *132*, 16141–16146.

[16] a) R. Ananthula, T. Yamada, P. H. Taylor, *J. Phys. Chem. A* **2006**, *110*, 3559–3566; b) H. Jia, G. Nulaji, H. Gao, F. Wang, Y. Zhu, C. Wang, *Environ. Sci. Technol.* **2016**, *50*, 6310–6319.

[17] S. Ito, K. Koshino, K. Mikami, *Chem. Asian J.* **2018**, *13*, 830–837.

[18] K. Koshino, K. M. Kojima, I. McKenzie, S. Ito, *Angew. Chem. Int. Ed.* **2021**, *60*, 24034–24038; *Angew. Chem.* **2021**, *133*, 24236–24240.

[19] R. M. Macrae, I. D. Reid, J.-U. von Schütz, K. Nagamine, *Physica B* **2000**, *289–290*, 616–619.

[20] a) D. Yu, P. W. Percival, J.-C. Brodovitch, S.-K. Leung, R. F. Kiefl, K. Venkateswaran, S. F. J. Cox, *Chem. Phys.* **1990**, *142*, 229–236; b) S. F. J. Cox, T. A. Claxton, M. C. R. Simons, *Radia. Phys. Chem.* **1986**, *28*, 107–113; c) E. Roduner, I. D. Reid, *Isr. J. Chem.* **1989**, *29*, 3–11.

[21] P. W. Percival, B. Addison-Jones, J.-C. Brodovitch, S. Sun-Mack, *Appl. Magn. Reson.* **1996**, *11*, 315–323.

[22] a) I. D. Reid, T. Azuma, E. Roduner, *Nature* **1990**, *345*, 328–330. See also:; b) M. Heming, *Z. Phys. Chem. Neue Folge* **1987**, *151*, 35–50.

[23] M. Mozafari, J.-C. Brodovitch, L. Chandrasena, P. W. Percival, *J. Phys. Chem. A* **2016**, *120*, 8521–8528.

[24] I. McKenzie, R. Scheuermann, I. Tucker, *Phys. Chem. Chem. Phys.* **2017**, *19*, 9551–9557.

[25] E. Niecke, A. Fuchs, F. Baumeister, M. Nieger, W. W. Schoeller, *Angew. Chem. Int. Ed. Engl.* **1995**, *34*, 555–557; *Angew. Chem.* **1995**, *107*, 640–642.

[26] H. Sugiyama, S. Ito, M. Yoshifuji, *Angew. Chem. Int. Ed.* **2003**, *42*, 3802–3804; *Angew. Chem.* **2003**, *115*, 3932–3934.

[27] a) S. Ito, *Tetrahedron Lett.* **2018**, *59*, 1–13; b) S. Ito, *Chem. Rec.* **2018**, *18*, 445–458.

[28] a) S. Ito, Y. Ueta, T. T. T. Ngo, M. Kobayashi, D. Hashizume, J.-i. Nishida, Y. Yamashita, K. Mikami, *J. Am. Chem. Soc.* **2013**, *135*, 17610–17616; b) Y. Ueta, K. Mikami, S. Ito, *Angew. Chem. Int. Ed.* **2016**, *55*, 7525–7529; *Angew. Chem.* **2016**, *128*, 7651–7655; c) S. Ito, Y. Torihata, K. Mikami, *ChemistrySelect* **2016**, *1*, 3310–3315.

[29] S. Ito, J. Miura, N. Morita, M. Yoshifuji, A. J. Arduengo, III, *Inorg. Chem.* **2009**, *48*, 8063–8065.

[30] Y. Ueta, K. Mikami, S. Ito, *Inorg. Chem.* **2015**, *54*, 8778–8785.

[31] I. McKenzie, J.-C. Brodovitch, P. W. Percival, T. Ramnial, J. A. C. Clyburne, *J. Am. Chem. Soc.* **2003**, *125*, 11565–11570.

[32] a) A. Mitra, J.-C. Brodovitch, C. Krempner, P. W. Percival, P. Vyas, R. West, *Angew. Chem. Int. Ed.* **2010**, *49*, 2893–2895; *Angew. Chem.* **2010**, *122*, 2955–2957; b) B. M. McCollum, J.-C. Brodovitch, J. A. C. Clyburne, P. W. Percival, R. West, *Physica B* **2009**, *404*, 940–942.

[33] Z. Wu, M. V. Barnabas, J. M. Stadlbauer, K. Venkateswaran, G. B. Porter, D. C. Walker, *J. Am. Chem. Soc.* **1991**, *113*, 9096–9099.

[34] T. Takayanagi, S. Koido, *Comp. Theor. Chem.* **2017**, *1115*, 4–12.

[35] J. Rosenboom, L. Chojetzki, T. Suhrbier, J. Rabeah, A. Villinger, R. Wustrack, J. Bresien, A. Schulz, *Chem. Eur. J.* **2022**, *28*, e202200624.

[36] S. Ito, H. Akama, Y. Ueta, I. McKenzie, K. M. Kojima, *Bull. Chem. Soc. Jpn.* **2021**, *94*, 2970–2972.

Manuscript received: March 17, 2022
Accepted manuscript online: June 14, 2022
Version of record online: July 25, 2022